Available online at www.sciencedirect.com
ScienceDirect
International Journal of Heat and Mass Transfer 50 (2007) 2182–2189
International Journal of HEAT and MASS TRANSFER
www.elsevier.com/locate/ijhmt

Forced convection heat transfer in microchannel heat sinks

Chien-Hsin Chen *

Department of Mechanical Design Engineering, National Formosa University, Huwei, Yunlin 632, Taiwan

Received 18 November 2005; received in revised form 1 November 2006
Available online 22 December 2006

Abstract

This paper presents an analysis of forced convection heat transfer in microchannel heat sinks for electronic system cooling. In view of the small dimensions of the microstructures, the microchannel is modeled as a fluid-saturated porous medium. Numerical solutions are obtained based on the Forchheimer–Brinkman-extended Darcy equation for the fluid flow and the two-equation model for heat transfer between the solid and fluid phases. The velocity field in the microchannel is first solved by a finite-difference scheme, and then the energy equations governing the solid and fluid phases are solved simultaneously for the temperature distributions. Also, analytical expressions for the velocity and temperature profiles are presented for a simpler flow model, i.e., the Brinkman-extended Darcy model. This work attempts to perform a systematic study on the effects of major parameters on the flow and heat transfer characteristics of forced convection in the microchannel heat sink. The governing parameters of engineering importance include the channel aspect ratio (α_s), inertial force parameter (Γ), porosity (ε), and the effective thermal conductivity ratio (k_r). The velocity profiles of the fluid in the microchannel, the temperature distributions of the solid and fluid phases, and the overall Nusselt number are illustrated for various values of the problem parameters. It is found that the fluid inertia force alters noticeably the dimensionless velocity distribution and the fluid temperature distribution, while the solid temperature distribution is almost insensitive to the fluid inertia. Moreover, the overall Nusselt number increases with increasing the values of α_s and ε, while it decreases with increasing k_r.

Keywords: Microchannel heat sinks; Forced convection; Electronics cooling

1. Introduction

Micro-scale heat transfer has received much interest as the size of the devices decreases, such as in electronic equipments, since the amount of heat that needs to be dissipated per unit area increases. The performance of these devices is directly related to the temperature; therefore it is a crucial issue to maintain the electronics at acceptable temperature levels. Microchannel heat sinks have become known as one of the effective cooling techniques, evidently first introduced by Tuckerman and Pease [1,2] for electronics cooling. A water-cooled integral heat sink for silicon integrated circuits has been designed and tested. With laminar flow in mind, they made a test section which achieved a power density of 790 W/cm^2 with a maximum substrate temperature rise of 71 °C above the input water temperature. Inspired by the technique developed by Tuckerman and Pease, much research has been conducted for microchannel heat sinks, as reviewed by Phillips [3]. The fin approach was employed in most of the previous studies. The fin approach is effective for the analysis of micro-scale heat transfer in many practical applications, and has been used recently to investigate the efficiency of micro-cell honeycombs in compact heat exchangers [4] and the design of cellar metal systems [5]. However, the fin approach assumes that the fluid temperature is uniform across the coolant flow, and this assumption makes its validity in a limited range. By using empirical correlations Knight et al. [6] evaluated the performance of a microchannel heat sink, and they reported that the total thermal resistance of a microchannel could be reduced by 35% compared to that obtained by Tuckerman and Pease with the fin approach [1].

* Tel.: +886 5 6315354; fax: +886 5 6363010.
E-mail address: chchen@nfu.edu.tw

0017-9310/$ - see front matter © 2006 Elsevier Ltd. All rights reserved.
doi:10.1016/j.ijheatmasstransfer.2006.11.001

Nomenclature

a	wetted area per volume
$\widetilde{Bi}$	equivalent Biot number, $haH^2/(1-\varepsilon)k_s$
c_f	heat capacity of fluid
C	inertial force coefficient
Da	Darcy number, K/H^2
D_h	hydraulic diameter of channel
h	interstitial heat transfer coefficient
$\bar{h}$	overall heat transfer coefficient
H	channel height
k_f	thermal conductivity of fluid
k_{fe}	effective thermal conductivity of fluid
k_r	effective thermal conductivity ratio, $\varepsilon k_f/(1-\varepsilon)k_s$
k_s	thermal conductivity of solid
k_{se}	effective thermal conductivity of solid
K	permeability
L	length of heat sink
$\dot{m}$	mass flow rate
$\overline{Nu}$	overall Nusselt number, $\bar{h}H/k_f$
p	pressure
q_w	heat flux over the bottom surface
t	thickness of the channel plate
T	temperature
u	velocity
u_D	Darcy velocity, $-(K/\varepsilon\mu_f)\mathrm{d}\langle p\rangle_f/\mathrm{d}x$
U	dimensionless velocity
w_c	width of channel
W	width of heat sink
Y	dimensionless vertical coordinate, y/H
$\langle\rangle_f$	volume-averaged value over fluid region
$\langle\rangle_s$	volume-averaged value over solid region

Greek symbols

α_s	aspect ratio of microchannel, H/w_c
Γ	inertial force parameter, $\rho_f u_D CK/\varepsilon\mu_f$
ε	porosity
θ	dimensionless temperature
μ_f	viscosity of fluid
ρ_f	density of fluid

Subscripts

f	fluid
m	mean value
s	solid
w	wall

Alternatively, in view of the small dimensions of the microstructures, Koh and Colony [7] modeled the microchannels as a porous medium by using Darcy's law to describe the flow. Later, Tien and Kuo [8] analyzed convection heat transfer in microstructures by using the Brinkman-extended Darcy model for fluid flow to account for the boundary effect. More recently, Kim and Kim [9] and Kim et al. [10] have presented analytical solutions for velocity and temperature distributions for forced convection in microchannel heat sinks by using the Brinkman-extended Darcy equation for the fluid flow. However, when the porous medium model is employed it is more reasonable to describe the fluid flow based on a more general flow model (see, for example, [11–13]) to account for the fluid inertia force. To the author's knowledge the analysis of flow and heat transfer in a microchannel heat sink using porous medium approach based on a general flow model has not been available. Therefore, the purpose of this study is to carry out an analysis of forced convection in a microchannel heat sink with the porous medium approach based on a general flow model. To this end, the Forchheimer–Brinkman-extended Darcy equation proposed by Vafai and Tien [11] will be used in the present analysis for the flow field to include the effects of fluid inertia and the solid boundary. Also, the two-equation model is used for heat transfer. In the present formulation it is shown that the problem under consideration depends on four governing parameters, including the channel aspect ratio, porosity, the inertial force parameter, and the effective thermal conductivity ratio. A parametric study on the effects of these parameters on the flow and heat transfer characteristics is performed to illustrate the basic thermal behavior of the microchannel heat sink. Results for the velocity profiles of the coolant flow, the temperature distributions of the solid and fluid phases, and the overall Nusselt number are presented for representative values of the governing parameters.

2. Mathematical formulation

Consider the problem of forced convective flow through a microchannel heat sink as shown in Fig. 1, heat is removed primarily by conduction through the solid and then dissipated away by convection of the cooling fluid in

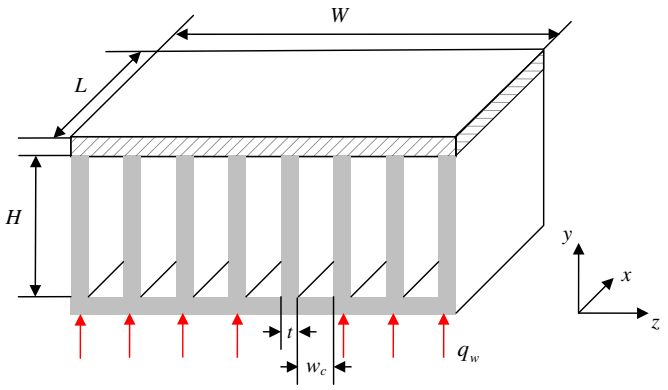

Fig. 1. Schematic of the microchannel heat sink.

the microchannel. Each channel has a height H, length L, width w_c, and the thickness of the channel plate is t. The direction of fluid flow is parallel to the x-axis. The bottom surface ($y = 0$) is uniformly heated with a constant heat flux and the top surface ($y = H$) is well insulated. Since the porous medium approach without entrance effect has been shown to predict well the flow and thermal characteristics of microchannel heat sinks [14]; to simplify the analysis, the flow is assumed to be laminar and both hydrodynamically and thermally fully developed. Also, the thermal physical properties are assumed to be constant. To relax the constant-fluid temperature assumption along the height of the channel wall in the fin approach, in the present analysis the microchannel heat sink is modeled as a fluid-saturated porous medium [8], as shown in Fig. 2. The Forchheimer–Brinkman-extended Darcy equation proposed by Vafai and Tien [11] for the fluid flow and the volume-averaged two-equation model [8] for heat transfer are used in this study. The governing equations and the corresponding boundary conditions can be expressed as

$$-\frac{\mathrm{d}}{\mathrm{d}x}\langle p\rangle_{\mathrm{f}} + \mu_{\mathrm{f}}\frac{\mathrm{d}^2}{\mathrm{d}y^2}\langle u\rangle_{\mathrm{f}} - \frac{\mu_{\mathrm{f}}}{K}\varepsilon\langle u\rangle_{\mathrm{f}} - \rho_{\mathrm{f}}C\langle u\rangle_{\mathrm{f}}^2 = 0 \tag{1}$$

$$k_{\mathrm{se}}\frac{\partial^2\langle T\rangle_{\mathrm{s}}}{\partial y^2} = ha(\langle T\rangle_{\mathrm{s}} - \langle T\rangle_{\mathrm{f}}) \tag{2}$$

$$\varepsilon\rho_{\mathrm{f}}c_{\mathrm{f}}\langle u\rangle_{\mathrm{f}}\frac{\partial\langle T\rangle_{\mathrm{f}}}{\partial x} = ha(\langle T\rangle_{\mathrm{s}} - \langle T\rangle_{\mathrm{f}}) + k_{\mathrm{fe}}\frac{\partial^2\langle T\rangle_{\mathrm{f}}}{\partial y^2} \tag{3}$$

$$\langle u\rangle_{\mathrm{f}} = 0 \quad \text{at } y = 0, H \tag{4}$$

$$\langle T\rangle_{\mathrm{s}} = \langle T\rangle_{\mathrm{f}} = T_{\mathrm{w}} \quad \text{at } y = 0 \tag{5}$$

$$\frac{\partial\langle T\rangle_{\mathrm{s}}}{\partial y} = \frac{\partial\langle T\rangle_{\mathrm{f}}}{\partial y} = 0 \quad \text{at } y = H \tag{6}$$

where the bracket $\langle\rangle$ represents a volume-averaged value, and K, C, ε, k_{se}, h, a, and k_{fe} are the permeability, inertial force coefficient, porosity, effective thermal conductivity of solid, interstitial heat transfer coefficient, wetted area per volume, and effective thermal conductivity of the fluid, respectively. For the rectangular microchannel heat sink, the porosity and the wetted area per volume can be expressed as

$$\varepsilon = \frac{w_c}{w_c + t}, \quad a = \frac{2}{w_c + t} \tag{7}$$

The effective thermal conductivities can be written as [9]

$$k_{\mathrm{se}} = (1-\varepsilon)k_{\mathrm{s}}, \quad k_{\mathrm{fe}} = \varepsilon k_{\mathrm{f}} \tag{8}$$

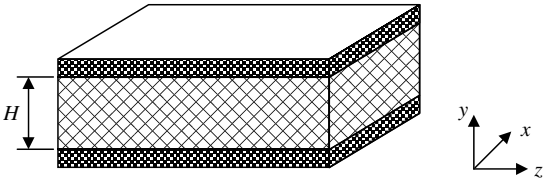

Fig. 2. The equivalent porous medium.

where k_{s} and k_{f} are thermal conductivity of solid and fluid, respectively.

To solve the governing equations (1)–(3), the permeability K and the interstitial heat transfer coefficient h should be determined in advance. For the present configuration, these parameters can be determined analytically through an approximation method devised by Kim [15]. It is assumed that the characteristics of pressure drop across and heat transfer from the fins under consideration can be approximated as those found for the Poiseuille flow between two infinite parallel plates that are subject to a constant heat flux. Then the velocity and temperature distributions can be obtained easily as

$$u_{\mathrm{f}} = \frac{w_c^2}{2\mu_{\mathrm{f}}}\left(-\frac{\mathrm{d}p}{\mathrm{d}x}\right)\left[\left(\frac{z}{w_c}\right) - \left(\frac{z}{w_c}\right)^2\right] \tag{9}$$

$$T_{\mathrm{f}} = \frac{q''w_c}{k_{\mathrm{f}}}\left[-\left(\frac{z}{w_c}\right)^4 + 2\left(\frac{z}{w_c}\right)^3 - \left(\frac{z}{w_c}\right)\right] + T_{\mathrm{w}} \tag{10}$$

Apply the volume averaging technique to get

$$\langle u\rangle_{\mathrm{f}} = \frac{1}{V_{\mathrm{f}}}\int_{V_{\mathrm{f}}} u\mathrm{d}V = \frac{w_c^2}{12\mu_{\mathrm{f}}}\left(-\frac{\mathrm{d}p}{\mathrm{d}x}\right) \tag{11}$$

$$\langle T\rangle_{\mathrm{f}} = \frac{1}{V_{\mathrm{f}}}\int_{V_{\mathrm{f}}} T\mathrm{d}V = T_{\mathrm{w}} - \frac{w_c^2}{10\alpha}\langle u\rangle_{\mathrm{f}}\frac{\mathrm{d}T_{\mathrm{f,m}}}{\mathrm{d}x} \tag{12}$$

Using these expressions together with the definition of the permeability and the interstitial heat transfer coefficient, it is found that

$$K = \frac{\varepsilon\mu_{\mathrm{f}}}{-(\mathrm{d}p/\mathrm{d}x)}\langle u\rangle_{\mathrm{f}} = \frac{\varepsilon w_c^2}{12} \tag{13}$$

$$h = \frac{q''}{T_{\mathrm{w}} - \langle T\rangle_{\mathrm{f}}} = \frac{5k_{\mathrm{f}}}{w_c} \tag{14}$$

To proceed, we introduce the following non-dimensional variables

$$Y = \frac{y}{H}, \quad U = \frac{\langle u\rangle_{\mathrm{f}}}{u_{\mathrm{D}}}, \quad \theta_{\mathrm{f}} = \frac{\langle T\rangle_{\mathrm{f}} - T_{\mathrm{w}}}{\frac{q_{\mathrm{w}}H}{(1-\varepsilon)k_{\mathrm{s}}}}, \quad \theta_{\mathrm{s}} = \frac{\langle T\rangle_{\mathrm{s}} - T_{\mathrm{w}}}{\frac{q_{\mathrm{w}}H}{(1-\varepsilon)k_{\mathrm{s}}}} \tag{15}$$

where $u_{\mathrm{D}} = -\frac{K}{\varepsilon\mu_{\mathrm{f}}}\frac{\mathrm{d}\langle p\rangle_{\mathrm{f}}}{\mathrm{d}x}$ is the Dacian convective velocity. For the fully developed flow subjected to a constant heat flux, it is known that

$$\frac{\partial\langle T\rangle_{\mathrm{f}}}{\partial x} = \frac{\partial\langle T\rangle_{\mathrm{s}}}{\partial x} = \frac{\mathrm{d}T_{\mathrm{w}}}{\mathrm{d}x} = \text{constant} \tag{16}$$

and the energy balance requires that

$$q_{\mathrm{w}} = \varepsilon\rho_{\mathrm{f}}c_{\mathrm{f}}u_{\mathrm{m}}H\frac{\partial\langle T\rangle_{\mathrm{f}}}{\partial x} \tag{17}$$

Substituting Eq. (15) into Eqs. (1)–(6) along with the use of Eqs. (16) and (17), one can get the following set of dimensionless governing equations and boundary conditions:

$$\frac{Da}{\varepsilon}\frac{\mathrm{d}^2U}{\mathrm{d}Y^2} - \Gamma U^2 - U + 1 = 0 \tag{18}$$

$$\frac{\mathrm{d}^2\theta_s}{\mathrm{d}Y^2} - \widetilde{B}i(\theta_s - \theta_f) = 0 \tag{19}$$

$$k_r\frac{\mathrm{d}^2\theta_f}{\mathrm{d}Y^2} + \widetilde{B}i(\theta_s - \theta_f) - SU = 0 \tag{20}$$

$$U = 0 \quad \text{at } Y = 0, 1 \tag{21}$$

$$\theta_s = \theta_f = 0 \quad \text{at } Y = 0 \tag{22}$$

$$\frac{\mathrm{d}\theta_s}{\mathrm{d}Y} = \frac{\mathrm{d}\theta_f}{\mathrm{d}Y} = 0 \quad \text{at } Y = 1 \tag{23}$$

where

$$Da = \frac{K}{H^2}, \quad \Gamma = \frac{\rho_f u_D C K}{\varepsilon\mu_f} \tag{24}$$

are the Darcy number and the inertial force parameter, respectively. The parameter S introduced in Eq. (20) is given by

$$S = \frac{1}{\int_0^1 U\mathrm{d}Y} \tag{25}$$

The parameters k_r and $\widetilde{B}i$ appearing in Eqs. (19) and (20) are the effective thermal conductivity ratio and the equivalent Biot number in porous medium model, respectively, and can be represented as

$$k_r = \frac{k_{fe}}{k_{se}} = \frac{\varepsilon k_f}{(1-\varepsilon)k_s} \tag{26}$$

and

$$\widetilde{B}i = \frac{haH^2}{k_{se}} = 10k_r\alpha_s^2 \tag{27}$$

where α_s is the aspect ratio of microchannel, $\alpha_s = H/w_c$. As the porous medium approach is adopted, the thermal energy transported by the fluid as it moves past a given cross section is

$$\dot{m}c_f\langle T\rangle_{f,m} = \int_{A_c}\rho_f\langle u\rangle_f c_f\langle T\rangle_f\mathrm{d}A$$

where $\dot{m}$ is the mass flow rate and $\langle T\rangle_{f,m}$ is the bulk mean fluid temperature using volume-averaged values. For constant-fluid properties,

$$\langle T\rangle_{f,m} = \frac{1}{u_m A_c}\int_{A_c}\langle u\rangle_f\langle T\rangle_f\mathrm{d}A \tag{28}$$

In a dimensionless form, the bulk mean fluid temperature is given by

$$\theta_{f,m} = \frac{\langle T\rangle_{f,m} - T_w}{\frac{q_w H}{(1-\varepsilon)k_s}} = \frac{\int_0^1 U\theta_f\mathrm{d}Y}{\int_0^1 U\mathrm{d}Y} \tag{29}$$

Heat transfer result can be represented by the overall Nusselt number, which is defined as

$$\overline{Nu} = \frac{\bar{h}H}{k_f} \tag{30}$$

where the overall heat transfer coefficient is defined as

$$\bar{h} = \frac{q_w}{T_w - T_{f,m}} \tag{31}$$

Here, $T_{f,m}$ is the conventional bulk mean temperature and can be expressed as

$$T_{f,m} = \frac{1}{u_m A_c}\int_{A_c} u_f T_f\mathrm{d}A \tag{32}$$

To account for the difference between the conventional bulk mean temperature and the bulk mean temperature defined in Eq. (28), proper correction for Eq. (28) can be made by using the general method suggested by Kim et al. [16]. They considered a certain volume filled with solid and fluid phases, inside this volume u_f and T_f can be decomposed into two terms: volume-averaged value and spatial variation:

$$u_f = \langle u\rangle_f + \tilde{u}_f \tag{33}$$

$$T_f = \langle T\rangle_f + \widetilde{T}_f \tag{34}$$

where $\langle\rangle_f$ denotes the mean value and $\sim$ indicates the variation from the mean value. Substituting Eqs. (34) and (35) into Eq. (32) leads to

$$T_{f,m} = \langle T\rangle_{f,m} + \frac{1}{u_m A_c}\int_{A_c}\tilde{u}_f\widetilde{T}_f\mathrm{d}A \tag{35}$$

For the present configuration, spatial variations of the velocity and temperature profiles can be expressed as

$$\tilde{u}_f = u_m\left[-6\left(\frac{z}{w_c}\right)^2 + 6\left(\frac{z}{w_c}\right) - 1\right] \tag{36}$$

$$\widetilde{T}_f = \frac{q''w_c}{k_f}\left[-\left(\frac{z}{w_c}\right)^4 + 2\left(\frac{z}{w_c}\right)^3 - \left(\frac{z}{w_c}\right) + \frac{1}{5}\right] \tag{37}$$

Substitute Eqs. (36) and (37) into Eq. (35) and perform the integration to obtain

$$T_{f,m} = \langle T\rangle_{f,m} - \frac{3}{70}\frac{q''w_c}{k_f} \tag{38}$$

Inserting Eq. (38) into Eq. (31) results in

$$\bar{h} = \left[-\frac{H\theta_{f,m}}{(1-\varepsilon)k_s} + \frac{3}{140}\frac{w_c^2}{k_f\varepsilon H}\right]^{-1} \tag{39}$$

Then, the overall Nusselt number for the microchannel heat sink can be represented by

$$\overline{Nu} = \frac{\bar{h}H}{k_f} = -\frac{\varepsilon}{k_r\theta_{f,m} - \frac{3}{140\alpha_s^2}} \tag{40}$$

3. Results and discussion

When the inertia term is neglected (i.e., $\Gamma = 0$), Eq. (1) reduces to the Brinkman-extended Darcy equation which is a linear one. For this case, by following a procedure described by Kim and Kim [9] analytical solutions for the velocity distribution of the fluid flow and the temperature

distributions of the solid and fluid phases are obtained as follows:

$$U(Y) = A\sinh\left(\sqrt{\frac{\varepsilon}{Da}}Y\right) - \cosh\left(\sqrt{\frac{\varepsilon}{Da}}Y\right) + 1 \tag{41}$$

$$\theta_f = \frac{-S}{1+k_r}\left\{-\frac{1}{2}Y^2 + C_1 Y + C_6 - C_3\cosh\left(\sqrt{\frac{\widetilde{B}i(1+k_r)}{k_r}}Y\right) - C_4\sinh\left(\sqrt{\frac{\widetilde{B}i(1+k_r)}{k_r}}Y\right) + C_7\left[\cosh\left(\sqrt{\frac{\varepsilon}{Da}}Y\right) + \frac{1-\cosh\left(\sqrt{\varepsilon/Da}\right)}{\sinh\left(\sqrt{\varepsilon/Da}\right)}\sinh\left(\sqrt{\frac{\varepsilon}{Da}}Y\right)\right]\right\} \tag{42}$$

$$\theta_s = -S\left\{\frac{Da}{\varepsilon}\left[\cosh\left(\sqrt{\frac{\varepsilon}{Da}}Y\right) + \frac{1-\cosh\left(\sqrt{\frac{\varepsilon}{Da}}\right)}{\sinh\left(\sqrt{\frac{\varepsilon}{Da}}\right)}\sinh\left(\sqrt{\frac{\varepsilon}{Da}}Y\right)\right] - \frac{1}{2}Y^2 + C_1 Y + C_2\right\} - k_r\theta_f \tag{43}$$

The coefficients appearing in the above expressions are given by

$$A = -\frac{1-\cosh(\sqrt{\varepsilon/Da})}{\sinh(\sqrt{\varepsilon/Da})}$$

$$C_1 = 1 - \sqrt{\frac{Da}{\varepsilon}}\frac{\cosh(\sqrt{\varepsilon/Da})-1}{\sinh(\sqrt{\varepsilon/Da})}$$

$$C_2 = -\frac{Da}{\varepsilon}$$

$$D_1 = \widetilde{B}i(1+k_r) - k_r\frac{\varepsilon}{Da}$$

$$C_3 = -\frac{k_r\frac{\varepsilon}{Da}}{\widetilde{B}i(1+k_r)D_1}$$

$$C_4 = \frac{N_1+N_2}{\widetilde{B}i(1+k_r)\sqrt{\frac{\widetilde{B}i(1+k_r)}{k_r}}\cosh\left(\sqrt{\frac{\widetilde{B}i(1+k_r)}{k_r}}\right)\sinh\left(\sqrt{\frac{\varepsilon}{Da}}\right)D_1}$$

$$C_5 = \frac{1}{D_1}$$

$$C_6 = \frac{1}{\widetilde{B}i(1+k_r)} - \frac{Da}{\varepsilon}$$

$$C_7 = \frac{Da}{\varepsilon} - \frac{1}{D_1}$$

$$N_1 = \widetilde{B}i(1+k_r)\sqrt{\frac{\varepsilon}{Da}}\left[1-\cosh\left(\sqrt{\frac{\varepsilon}{Da}}\right)\right]$$

$$N_2 = k_r\frac{\varepsilon}{Da}\sqrt{\frac{\widetilde{B}i(1+k_r)}{k_r}}\sinh\left(\sqrt{\frac{\varepsilon}{Da}}\right)\sinh\left(\sqrt{\frac{\widetilde{B}i(1+k_r)}{k_r}}\right)$$

It is noted here that for the case when the inertia effect is neglected the dimensionless velocity distribution, Eq. (41), is a function of ε/Da only. This implies that U is a function of the aspect ratio α_s only, since $\varepsilon/Da = 12\alpha_s^2$. On the other hand, the velocity profile depends not only on the aspect ratio but also on the inertial force parameter Γ when the fluid inertia is incorporated in the momentum equation. Now, since $d\langle p\rangle_f/dx = -\varepsilon\mu_f u_D/K$, the pressure drop $\Delta\langle p\rangle_f$ is obtained as

$$\Delta\langle p\rangle_f = \int_0^L \frac{d\langle p\rangle_f}{dx}dx = -\frac{12\mu_f u_D L}{w_c^2} \tag{44}$$

from which the friction factor can be given by

$$f = \frac{D_h\Delta\langle p\rangle_f}{\frac{1}{2}\rho_f u_m^2 L} = \frac{96}{Re(2A\sqrt{\frac{Da}{\varepsilon}}-1)}\left(\frac{\alpha_s}{\alpha_s+1}\right)^2 \tag{45}$$

where D_h is the hydraulic diameter of the microchannel and $Re = \rho_f u_m D_h/\mu_f$ is the Reynolds number.

For the more general flow situation, the full set of Eqs. (18)–(23) is solved numerically by the finite-difference method based on central differences, due to the nonlinear nature of the Forchheimer–Brinkman-extended Darcy equation. To access the accuracy of the numerical method, a comparison between analytical and numerical solutions has been made for the case when $\Gamma = 0$, and an excellent agreement has been found. Next, quantities of interest including the dimensionless velocity distributions, the temperature distributions of the solid and fluid phases, and the overall Nusselt number are illustrated for representative values of the governing parameters in Figs. 3–9.

Fig. 3 represents the dimensionless velocity profiles for different values of the inertial force parameter Γ (characterizing the fluid inertia effect) with a channel aspect ratio of $\alpha_s = 1$. The inertial effect tends to reduce the dimensionless velocity, i.e. increasing the value of Γ will produce a reduction in the velocity for a given value of α_s, as shown in Fig. 3. This is because that the last term on the left-hand side of Eq. (1), commonly known as the Forchheimer or Ergun inertial term, accounts for the additional pressure drop and the form drag due to the solid obstacles, and hence retards the momentum transport, which in turn reduces the fluid velocity in the channel. Since the fluid inertia effect may alter the velocity profiles considerably, we had better consider this effect by including the Ergun

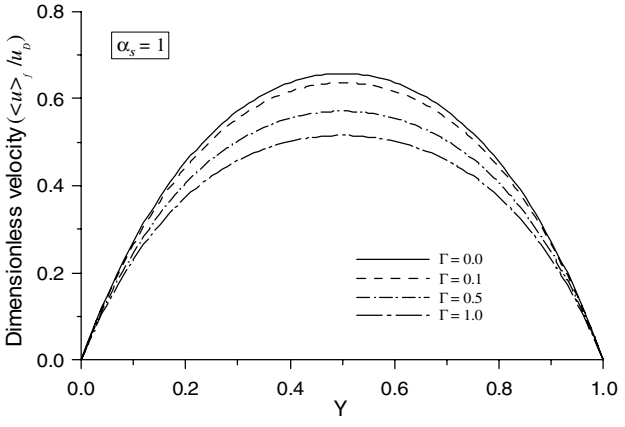

Fig. 3. Effects of inertial force parameter Γ on the velocity profiles for $\alpha_s = 1$.

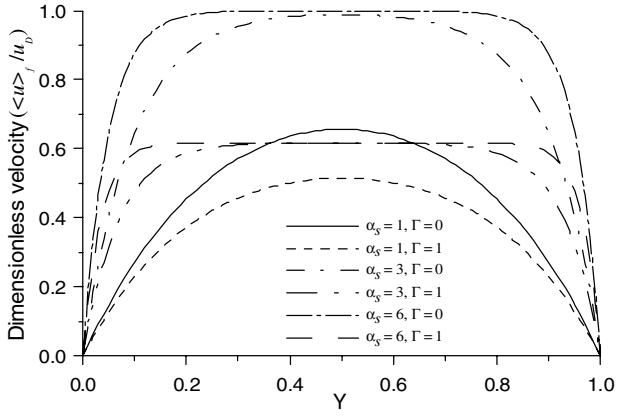

Fig. 4. Dimensionless velocity profiles for various values of α_s and Γ.

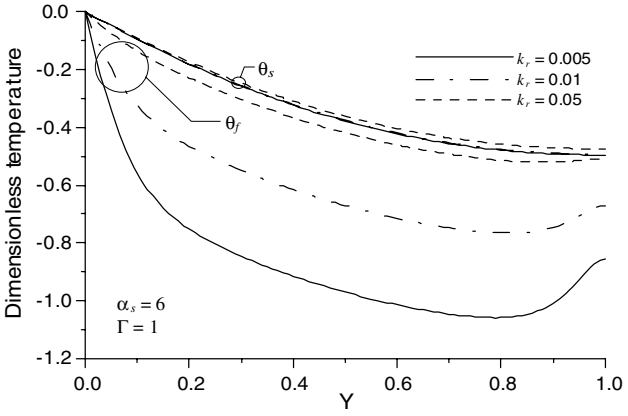

Fig. 7. Temperature profiles at selected values of k_r.

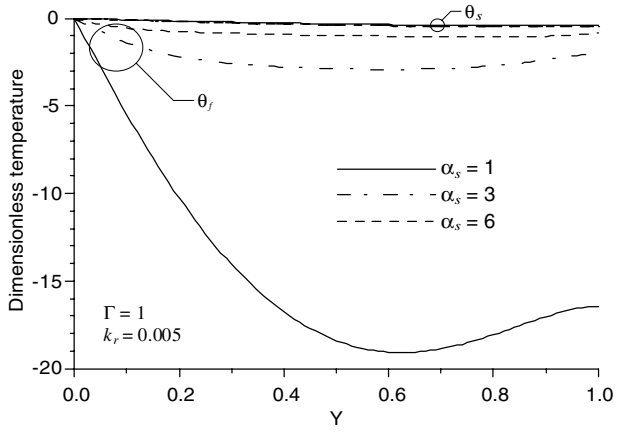

Fig. 5. Temperature profiles at selected values of α_s.

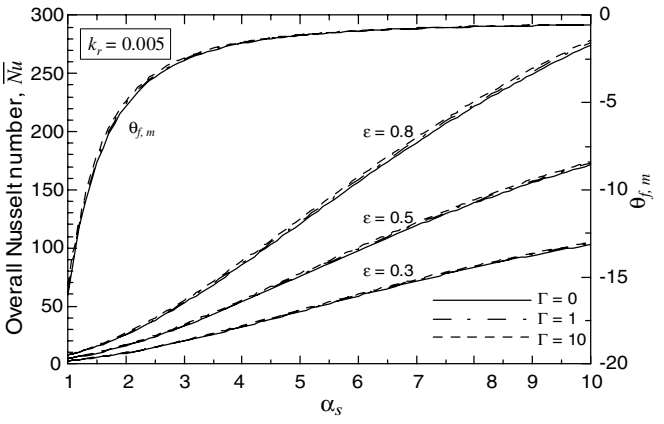

Fig. 8. Overall Nusselt number vs. α_s at selected values of ε and Γ.

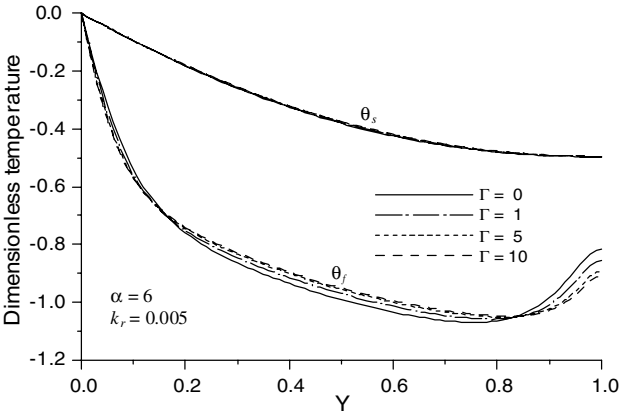

Fig. 6. Temperature profiles at selected values of Γ.

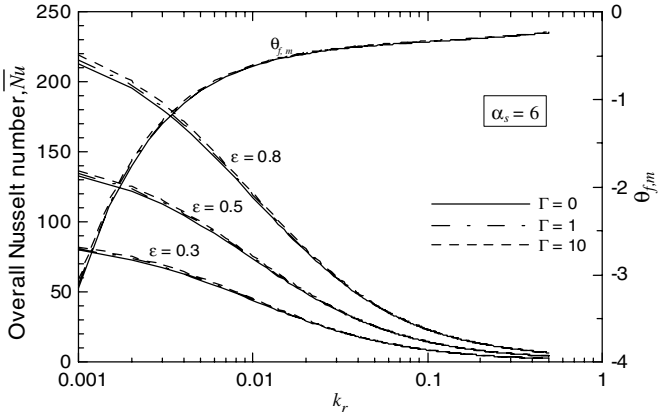

Fig. 9. Overall Nusselt number vs. k_r at selected values of ε and Γ.

inertial term in the analysis when the porous medium model is employed. Moreover, for $\alpha_s = 1$ the present calculations show that the change in the maximum velocity (occurring at the centerline, $Y = 0.5$) is about 3% for $\Gamma = 0.1$, 13% for $\Gamma = 0.5$, and 22% for $\Gamma = 1$. Calculations have also been carried out for several channel aspect ratios greater than unity and the results show that the influence of inertial force on the velocity is more pronounced as α_s becomes larger. The detailed results are not presented here for the sake of brevity. Generally, we may conclude that the inertial term needs to be considered for modeling the fluid flow when the inertial force parameter $\Gamma \geqslant 0.5$. Fig. 4 illustrates the dimensionless velocity profiles for various values of α_s with two values of Γ, i.e. 0 and 1. It

is evident that the decrease in the velocity due to the inertial effect becomes more significant for a larger aspect ratio. Also, it can be seen that for a specific value of Γ the region sensitive to the boundary effect increases as α_s decreases, which produces a rise in the deviation from the mean velocity. Therefore, the velocity distribution is more uniform for a larger value of α_s in a manner that the velocity distribution flattens as α_s increases.

The effects of various problem parameters on the temperature distributions of the fluid and solid phases are illustrated in Figs. 5–7. Fig. 5 demonstrates the effect of channel aspect ratio on the dimensionless temperature distributions of both phases for $\Gamma = 1$ and $k_r = 0.005$. An increase in the aspect ratio tends to increase the fluid temperature, while only slight effect of the aspect ratio is observed on the solid temperature. Also, it reveals clearly that the fluid temperature first rapidly decreases from its maximum value at the bottom wall ($Y = 0$), arrives at a minimum, and then increases more gradually to its value at the top wall. This phenomenon is more pronounced for a smaller value of α_s. On the other hand, the solid temperature with its maximum value at $Y = 0$ decreases slowly with increasing Y. It is noted that the tendency of temperature distribution displayed in Fig. 5 is similar to that presented in [9] for $\Gamma = 0$, in which the fluid flow is described by the Brinkman's model. Fig. 6 shows the solid and fluid temperature profiles at selected values of the inertial force parameter for $\alpha_s = 6$ and $k_r = 0.005$. The solid temperature is seen to be nearly insensitive to fluid inertia, while the fluid temperature distribution is affected appreciably by the fluid inertial force. As compared to the case of $\Gamma = 0$, a larger value of Γ results that the fluid temperature first decreases more rapidly with Y, following with a more gradual decrease to attain a minimum, and then increases more slowly to the top wall temperature. The computation shows that the inertia effect on the fluid temperature becomes appreciable when Γ is greater than unity (e.g. the maximum change in the fluid temperature due to inertia effect is about 5% for $\Gamma = 1$ and 11% for $\Gamma = 10$). Fig. 7 shows the effect of the effective thermal conductivity ratio k_r on the dimensionless temperature distributions. For specific values of aspect ratio ($\alpha_s = 6$) and inertial force parameter ($\Gamma = 1$), Fig. 7 reveals that an increase in k_r is found to increase the temperature of the fluid and solid phases. Moreover, the temperature difference between the solid and fluid phases increases as the effective thermal conductivity ratio decreases. This can be understood from the fact that the difference in temperature gradients between the phases increases as k_f/k_s decreases, which in turn gives rise to the increase in the temperature difference between the fluid and solid phases.

The overall Nusselt number is plotted against the channel aspect ratio at selected values of porosity and inertial force parameter for $k_r = 0.005$ in Fig. 8. It is found that the overall Nusselt number increases with increasing aspect ratio. As the channel aspect ratio increases, the temperature difference between the phases decreases (see Fig. 5), which leads to an increase in the interstitial heat transfer coefficient and hence the overall Nusselt number increases. For a given value of α_s, a larger porosity will produce a larger overall Nusselt number. This can be readily understood from the expression of the overall Nusselt number, Eq. (40). Although the fluid inertia affects appreciably the fluid temperature distribution, Fig. 8 displays that an increase in the inertial force parameter can only results in a small increase in the mean fluid temperature, which in turn increases slightly the overall Nusselt number. Fig. 9 represents the effect of the effective thermal conductivity ratio on the overall Nusselt number for $\alpha_s = 6$ at selected values of ε and Γ. It is clear from this figure that the overall Nusselt number decreases with increasing k_r. This behavior can be explained from the fact that the temperature difference between the solid and fluid phases decreases as k_r increases (see Fig. 7), which sequentially gives an increase in the overall Nusselt number. Again, the influence of inertial force on the mean fluid temperature and the overall Nusselt number is seen to be very limited.

4. Conclusions

In this work the problem of forced convection heat transfer in a microchannel heat sink has been investigated by modeling the microchannel as a fluid-saturated porous medium. The fluid flow is described by the Forchheimer–Brinkman-extended Darcy model and the two-equation model is used for heat transfer between the solid and fluid phases. Numerical solutions are obtained for the velocity profiles, the temperature distributions of the solid and fluid phases, and the overall Nusselt number. In addition, based on the Brinkman-extended Darcy model, analytical solutions are presented for the velocity and temperature profiles. The governing parameters of this problem include the channel aspect ratio, the inertial force parameter, porosity, and the effective thermal conductivity ratio. Effects of these parameters on the flow and heat transfer characteristics in the microchannel heat sink are examined. The solid temperature distribution is found to be practically insensitive to the fluid inertia force and the channel aspect ratio, while the dimensionless velocity distribution and the fluid temperature distribution depend on the inertial force parameter and the aspect ratio. More specific, in the present calculation the inertial effect is found to reduce significantly the velocity if the inertial force parameter $\Gamma \geqslant 0.5$, while this effect on the fluid temperature becomes appreciable when $\Gamma \geqslant 1$. The overall Nusselt number is found to increase with increasing the aspect ratio and porosity, whereas it decreases with increasing the effective thermal conductivity ratio. Furthermore, the effects of inertial force on the mean fluid temperature and the overall Nusselt number are found to be minor.

Acknowledgements

This work was partially supported by the National Science Council of Taiwan (Grant Number NSC

92-2212-E-150-020). The author is also grateful to Professor S.J. Kim (Korea Advanced Institute of Science and Technology) for his help.

References

[1] D.B. Tuckerman, R.F.W. Pease, High-performance heat sinking for VLSI, IEEE Electr. Dev. Lett. 2 (1981) 126–129.
[2] D.B. Tuckerman, R.F.W. Pease, Ultrahigh thermal conductance microstructures for integrated circuits, in: IEEE Proceedings of the 32nd Electronic Conference, 1982, pp. 145–149.
[3] R.J. Phillips, Microchannel heat sinks, in: A. Bar-Cohen, A.D. Krous (Eds.), Advances in Thermal Modeling of Electronic Components and Systems, vol. 2, ASME, New York, 1990.
[4] T.J. Lu, Heat transfer efficiency of metal honeycombs, Int. J. Heat Mass Transfer 42 (1999) 2031–2040.
[5] S. Gu, T.J. Lu, A.G. Evans, On the design of two-dimensional cellar metals for combined heat dissipation and structural load capacity, Int. J. Heat Mass Transfer 44 (2001) 2163–2175.
[6] R.W. Knight, J.S. Goodling, D.J. Hall, Optimal thermal design of forced convection heat sinks-analytical, ASME J. Electron. Packaging 113 (1991) 313–321.
[7] J.C.Y. Koh, R. Colony, Heat transfer of microstructures for integrated circuits, Int. Commun. Heat Mass Transfer 13 (1986) 89–98.
[8] C.L. Tien, S.M. Kuo, Analysis of forced convection in microstructures for electronic system cooling, in: Proceedings of the International Symposium Cooling Technology for Electronic Equipment, Honolulu, HI, 1987, pp. 217–226.
[9] S.J. Kim, D. Kim, Forced convection in microstructures for electronic equipment cooling, ASME J. Heat Transfer 121 (1999) 635–645.
[10] S.J. Kim, D. Kim, D.Y. Lee, On the local thermal equilibrium in micro channel heat sinks, Int. J. Heat Mass Transfer 43 (2000) 1735–1748.
[11] K. Vafai, C.L. Tien, Boundary and inertia effects on flow and heat transfer in porous media, Int. J. Heat Mass Transfer 24 (1981) 195–203.
[12] P. Poulikakos, K. Renken, Forced convection in a channel filled with porous medium, including the effects of flow inertia, variable porosity, and Brinkman friction, ASME J. Heat Transfer 109 (1987) 880–888.
[13] C.-H. Chen, Analysis on non-Darcy mixed convection from impermeable horizontal surfaces in porous media-the entire regime, Int. J. Heat Mass Transfer 40 (1997) 2993–2997.
[14] D. Kim, S.J. Kim, Compact modeling of fluid flow and heat transfer in straight fin heat sinks, ASME J. Electron. Packaging 126 (2004) 247–255.
[15] S.J. Kim, Methods for thermal optimization of microchannel heat sinks, Heat Transfer Eng. 25 (2004) 37–49.
[16] S.J. Kim, J.W. Yoo, S.P. Jang, Thermal optimization of a circular-sectored finned tube using a porous medium approach, ASME J. Heat Transfer 124 (2002) 1026–1033.